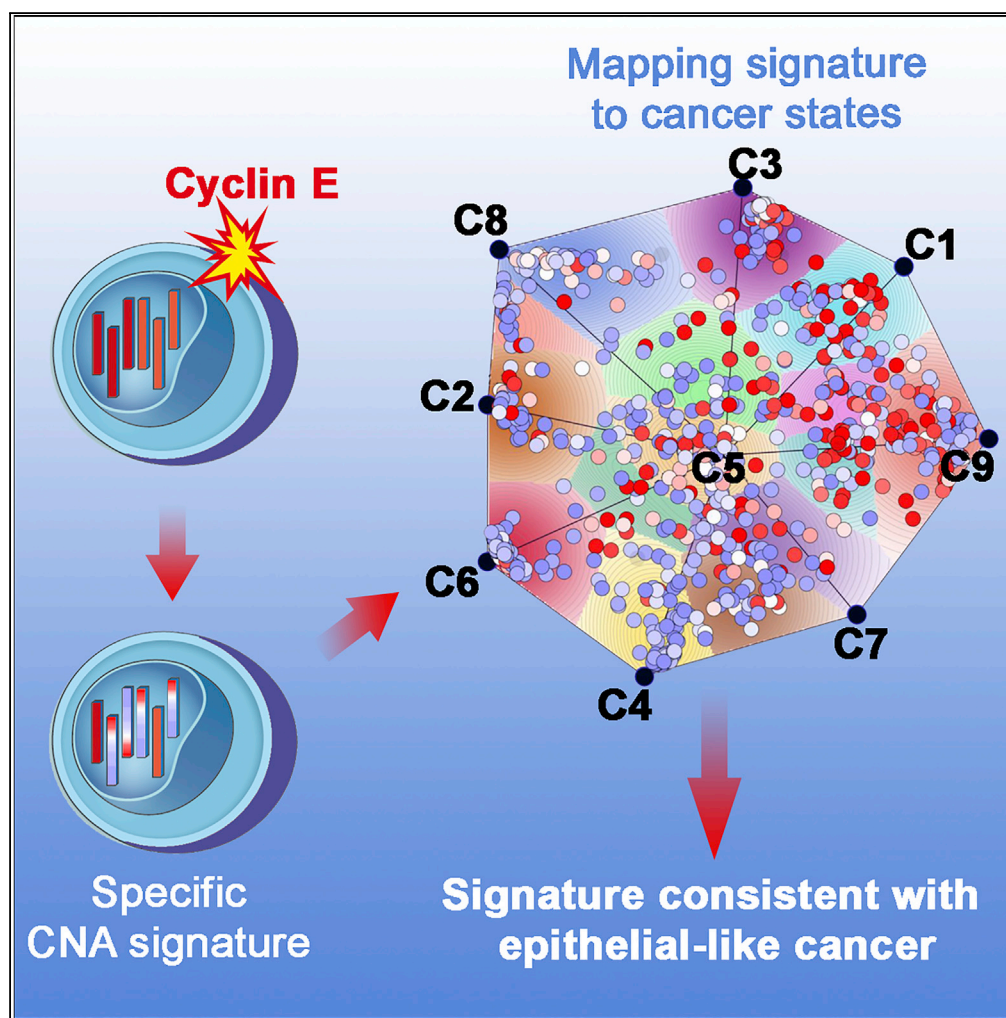


Article

Cyclin E Overexpression in Human Mammary Epithelial Cells Promotes Epithelial Cancer-Specific Copy Number Alterations



Servando Giraldez, Pablo Tamayo, Nathan Wineinger, William Kim, Steven I. Reed

sreed@scripps.edu

HIGHLIGHTS

Cyclin E overexpression produces a copy number alteration (CNA) signature

Cyclin E signature shows association with features of epithelial-like cancers

Cyclin E signature is reflected in altered patterns of transcription

Cyclin E signature resembles CNA profile in differentiated breast and ovarian cancers

Giraldez et al., iScience 19, 850–859
 September 27, 2019 © 2019
 The Authors.
<https://doi.org/10.1016/j.isci.2019.08.043>

Article

Cyclin E Overexpression in Human Mammary Epithelial Cells Promotes Epithelial Cancer-Specific Copy Number Alterations

Servando Giraldez,¹ Pablo Tamayo,^{2,3} Nathan Wineinger,⁴ William Kim,^{2,3} and Steven I. Reed^{1,5,*}

SUMMARY

Cyclin E, a key cell cycle regulatory protein, has been linked to oncogenesis when dysregulated. We have previously shown that overexpression of cyclin E causes replication stress, leading to failure to complete replication at specific chromosomal loci during S phase of the cell cycle. This in turn promotes chromosomal damage during anaphase. Here we show that non-transformed human mammary epithelial cell clones that survive such aberrant mitoses have a specific and reproducible pattern of chromosomal Copy Number Alterations (CNAs) that we have characterized and termed the cyclin E CNA signature. Using a number of computational approaches, we show that this signature resembles one specific CNA pattern enriched in differentiated epithelial-like tumors of the breast and ovary. Analysis of the CNA profile of these clones provides a potential mechanism for cyclin E-mediated oncogenesis.

INTRODUCTION

There are several lines of evidence from different models indicating that cyclin E deregulation causes replication stress in S phase and chromosome segregation errors in M phase, leading to genomic instability and cancer (Bartkova et al., 2006; Bortner and Rosenberg, 1997; Porter et al., 1997; Smith et al., 2006; Spruck et al., 1999). However, the mechanistic link between cyclin E-mediated genomic instability and tumorigenesis remains poorly understood. We hypothesized that cyclin E deregulation promotes oncogenesis by creating a specific pattern of Copy Number Alterations (CNAs).

In our previous work, we demonstrated that transient overexpression of cyclin E in non-transformed human mammary epithelial cells (HME1) causes failure to replicate specific genomic regions and resulting genomic instability (Teixeira et al., 2015). However, the degree of DNA damage incurred impeded clonal expansion of these cells, presumably due to p53-dependent checkpoint activation, and therefore prevented us from studying the effects of cyclin E overexpression on the genomic landscape during the early stages of cancer development. To circumvent this problem, an HME1 derivative cell line (HME1-E6) constitutively expressing the human papilloma virus (HPV) E6 protein, which promotes proteasomal degradation of p53 (Thomas et al., 1999), was constructed. As shown (Figure S1A), p53 levels are reduced in HME1-E6 cells relative to the parental cell line HME1. To test whether reduction of p53 levels confers resistance to DNA damage, we treated HME1 and HME1-E6 lines with the topoisomerase inhibitor etoposide and determined the level of apoptosis based on the appearance of cleaved PARP. Cleaved PARP was apparent in HME1 cells after 24 h, whereas HME1-E6 exhibited a similar level of cleaved PARP only after 48 h, suggesting that HME1-E6 cells are more resistant to DNA damage (Figure S1B). Using a second marker for apoptosis, Annexin V staining, similar results were obtained. Approximately 80% of HME1 cells stained positively after 24 h of etoposide treatment compared with 58% of HME1-E6 (Figure S1C). These data indicate that HME1-E6 is more resistant to DNA damage and therefore more likely to sustain clonal expansion after acute expression of cyclin E. This was confirmed when, after overexpressing cyclin E, we were able to obtain single-cell-derived populations bearing chromosomal deletions in regions defined as under-replicated in our previous study (Teixeira et al., 2015) (Figure 1A).

Transient Cyclin E Expression Produces a Specific CNA Signature in HME1-E6 Cells

To determine whether cyclin E expression produces a specific genome-wide CNA signature, Chromosomal Microarray (CMA) analysis was carried out on DNA from individual clones. CNA call analysis of the CMA

¹Department of Molecular Medicine, The Scripps Research Institute, La Jolla, CA 92037, USA

²Center for Cancer Target Discovery and Development (CTD²), UCSD Moores Cancer Center, La Jolla, CA 92093, USA

³Division of Medical Genetics, UCSD School of Medicine, La Jolla, CA 92093, USA

⁴The Scripps Translational Science Institute, La Jolla, CA 9203, USA

⁵Lead Contact

*Correspondence: sreed@scripps.edu

<https://doi.org/10.1016/j.isci.2019.08.043>



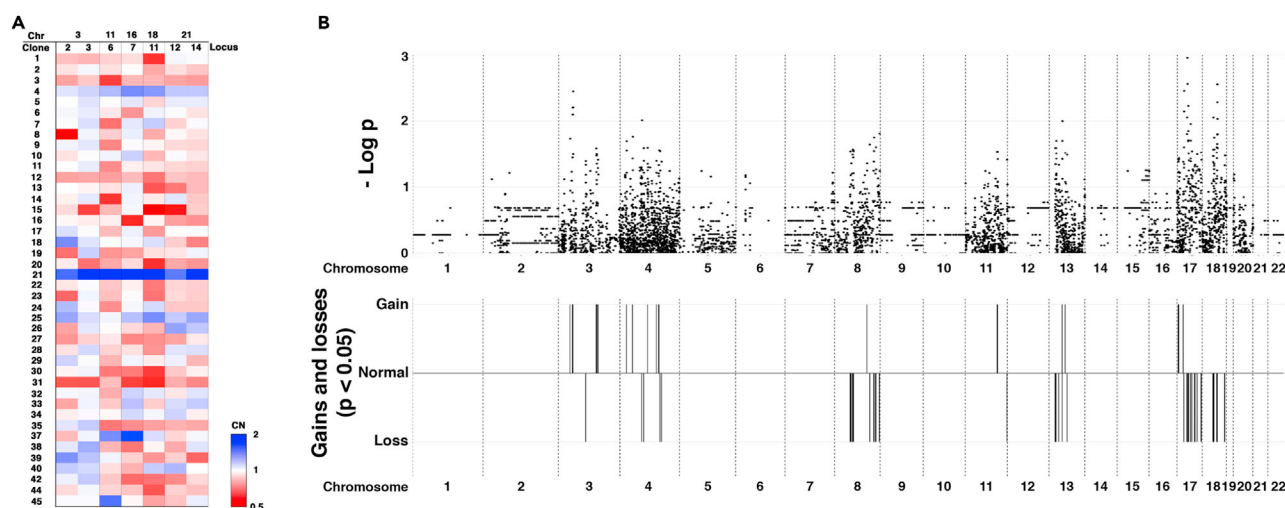


Figure 1. Chromosomal Analysis of HME1-E6 Clonal Populations of Transient Expression of Cyclin E

(A) Heatmap of CNAs determined by qPCR at some of loci identified in previous study (Teixeira et al., 2015). Forty-two cyclin E clones were analyzed and compared with the average of seven control clones. Blue, CNA gains; red CNA losses. Normalization to locus encoding α -tubulin. Intensity of color indicates magnitude of CNA.

(B) Transient cyclin E overexpression leads to characteristic CNA signature. CMA analysis of 12 cyclin E and 7 control clones. Data shown are based on CNA call analysis. Bottom plot shows gains (+1) and losses (−1) across 22 chromosomes for all CNAs with a p value ≤ 0.05 . Upper Manhattan plot shows significance as $-\log(p)$.

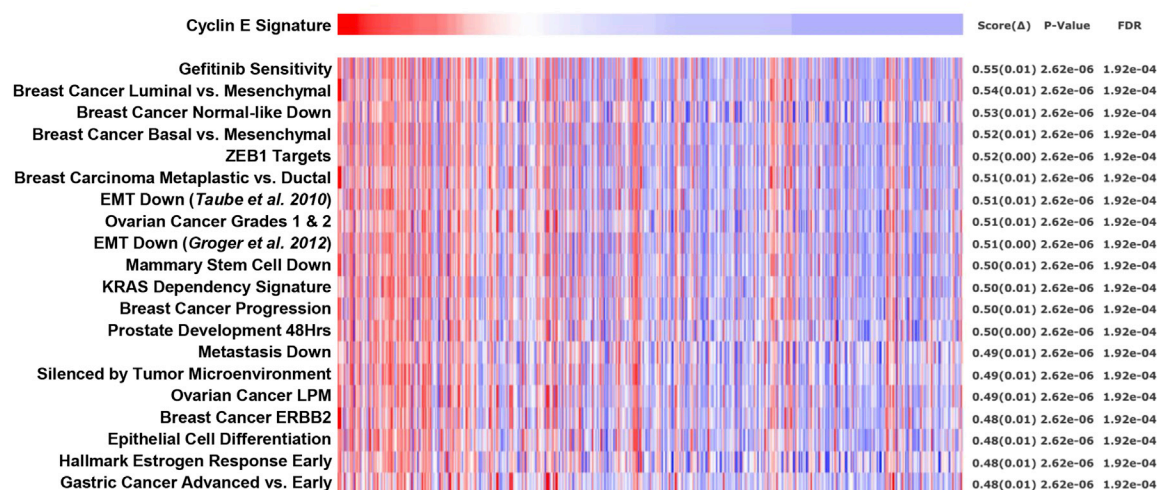
data from 12 cyclin E-overexpressing clones and 7 control clones (expressing GFP) was performed to generate a cyclin E-mediated CNA profile. The gains and losses are represented as a non-quantitative histogram, with significance indicated using a Manhattan plot, in Figure 1B. The normalized array data used to produce Figure 1B are shown in Table S1. As can be seen, cyclin E expression causes highly significant copy number increases and decreases relative to controls.

Relationship of the Cyclin E CNA Signature to Cancer States

To determine whether the cyclin E CNA profile is related to specific cancer states, we carried out an association analysis against cancer cell lines (The Cancer Cell Line Encyclopedia, CCLE [Barretina et al., 2012], and primary samples from the Pan-cancer The Cancer Genome Atlas, TCGA [Lawrence et al., 2014; Wang et al., 2016]) dataset. We defined a cyclin E CNA signature score for each cancer sample by adding all its observed cyclin E-mediated gains and losses weighted by an amount corresponding to the log of the inverse of its p value (Figure 1B) so that the most significant CNAs will have a higher contribution to the score (see Transparent Methods). Repeating this procedure for each sample allowed us to define a vector of cyclin E CNA scores for all CCLE and TCGA samples. Then we matched the signature scores against pathway (single-sample Gene Set Enrichment Analysis, GSEA) and protein expression profiles (Reverse Phase Protein Array, RPPA). To quantify the strength of association we used the Information Coefficient, which is an Information theoretic metric that provides a non-linear counterpart of the Pearson correlation coefficient (Joe, 1989; Kim et al., 2016). The goal of this analysis is to find genomic correlates of the cyclin E signature that will be informative, e.g., to assess the characteristics of samples with higher versus lower cyclin E signature scores. Interestingly, significant association was detected between the cyclin E signature and several epithelial-like gene sets from the Molecular Signatures Database (MsigDB [Joe, 1989; Kim et al., 2016; Liberzon, 2014; Liberzon et al., 2015; Liberzon et al., 2011]) (Figure 2, top). These top scoring gene sets include those representing ZEB1 targets, downregulation of the epithelial-mesenchymal transition (EMT), stem cell and metastasis, epithelial cell differentiation, ERBB2, EGFR inhibition sensitivity, and KRAS dependency. Consistent with this picture, the top scoring proteins included claudin, e-cadherin, HER2, and EGFR (Figure 2, bottom).

We then used the Oncogenic Positioning System (Onco-GPS), a data driven computational analysis that projects and clusters cancer samples onto a 2-dimensional reference map based on their most salient patterns of gene expression behavior (Kim et al., 2017). We took a variant of the global Onco-GPS map introduced in Kim et al. (2017) (Figure 3A) and used it to determine if samples with high cyclin E signature score

Cyclin E Signature — Top Pathway Associations



Cyclin E Signature — Top Protein Expression Associations

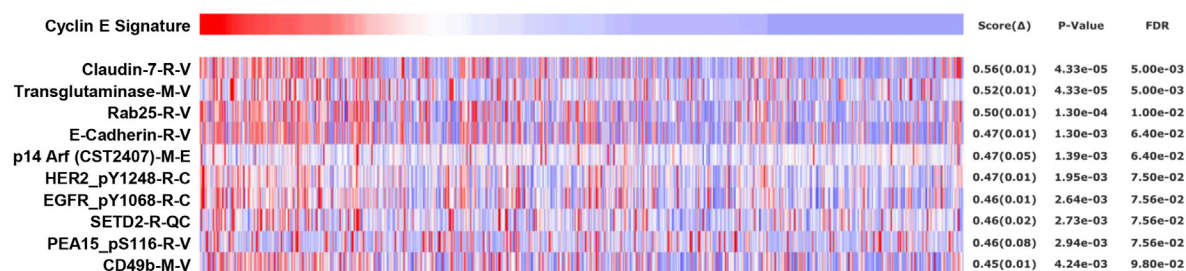


Figure 2. Pathway and Protein Association Analysis Indicates that Transient Cyclin E Overexpression Produces a Cellular State with Similarities to Differentiated Epithelial-like Tumors

Top 20 pathways and top 10 proteins associated with the cyclin E CNA signature. Top bar in the heatmaps shows the high-to-low sorted amplitude of the cyclin E CNA signature across 958 cell lines in the CCLE dataset. The top scoring gene sets and proteins are strongly consistent with relatively differentiated mammary carcinomas such as ductal and basal and not with less differentiated mesenchymal-like cancers, mammary stem cells, or non-malignant mammary tissue. Statistical significance of top-scoring features was assessed by an empirical permutation test, and its corresponding null distribution, false discovery rates (FDR) plus bootstrap estimates of the association metric confidence intervals.

were enriched in any specific previously determined cancer state. To carry out this analysis, we color-coded each of the CCLE cell lines (Kim et al., 2017). Consistent with the previous analysis, the cyclin E CNA signature was enriched primarily in epithelial-like cancer samples (Figure 3B). This is better appreciated if one compares the map shown in Figure 3B with the same map where the samples are color-coded to represent the enrichment in ZEB1 targets, shown on the left side of Figure 4A, which have higher expression in the top right side of the map, and provide a guide of where the most epithelial cancer states are located. When one compares this pattern (Figure 4A, left) against the pattern of cyclin E CNA signature scores (Figure 3B), one can observe an overlap that is indeed statistically significant when quantified by the Information Coefficient between those two patterns (IC:0.52, p value: 2.62×10^{-6} , Figure 2A). The cyclin E CNA signature was much lower in cancers that were less differentiated and had undergone EMT (Figure 4B). A similar trend was observed in the Pan-cancer TCGA samples where the samples that are projected onto the Onco-GPS epithelial states have often higher scores for the cyclin E CNA signature (Figure 5). These results are consistent with the idea that transient cyclin E overexpression in non-transformed mammary epithelial cells produces a CNA signature that appears to be enriched in differentiated epithelial cancer states.

Subsets of Clones Bearing the Cyclin E CNA Signature Show Properties Associated with Malignant Transformation

To determine whether the cyclin E CNA signature actually represents a cancer-like state, we tested whether clones analyzed in this study were capable of anchorage-independent growth or were resistant to

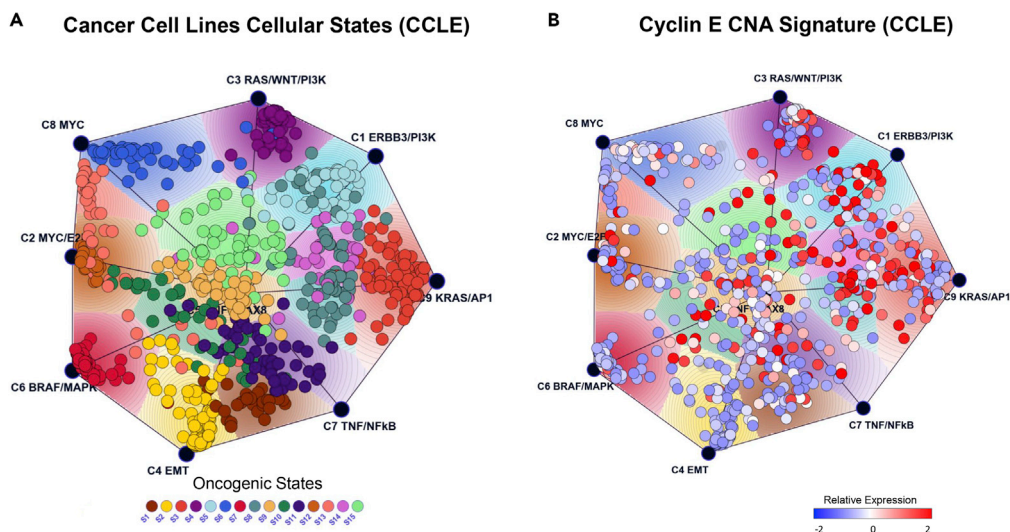


Figure 3. Onco-GPS Analysis Indicates that Transient Cyclin E Overexpression Produces a State with Similarities to Epithelial-like Cancers

(A) Onco-GPS map showing 15 cancer states (a variant of the map introduced in [Groger et al., 2012]).
 (B) Same map as in (A) but with the samples color-coded to show the expression of the cyclin E CNA signature.

apoptosis, properties associated with oncogenic transformation. The parental cell line, HME1-E6, and all 7 control clones could not form colonies in soft agar, whereas remarkably 2 out of 12 clones that had been subjected to transient cyclin E overexpression could (Figures 6A and 6B). Clearly not all cells in these clonal populations could form colonies, as compared with the positive control, a metastatic breast cancer-derived cell line. This indicates that additional genetic or epigenetic changes, existing as variants in the population, are necessary to support anchorage-independent growth. To gain more insight into the specific CNAs that might explain the behavior of these two clones, we carried out a genome-wide association study (GWAS) comparing them with the 10 clones incapable of anchorage-independent growth (Figure S2). The most salient characteristic found was amplification of a segment of Chromosome 8 containing the *c-Myc* oncogene. It is notable that *c-Myc* overexpression has been shown to be associated with anchorage-independent growth (Lyn-Cook et al., 1990; Telang et al., 1990; Valverius et al., 1990). In

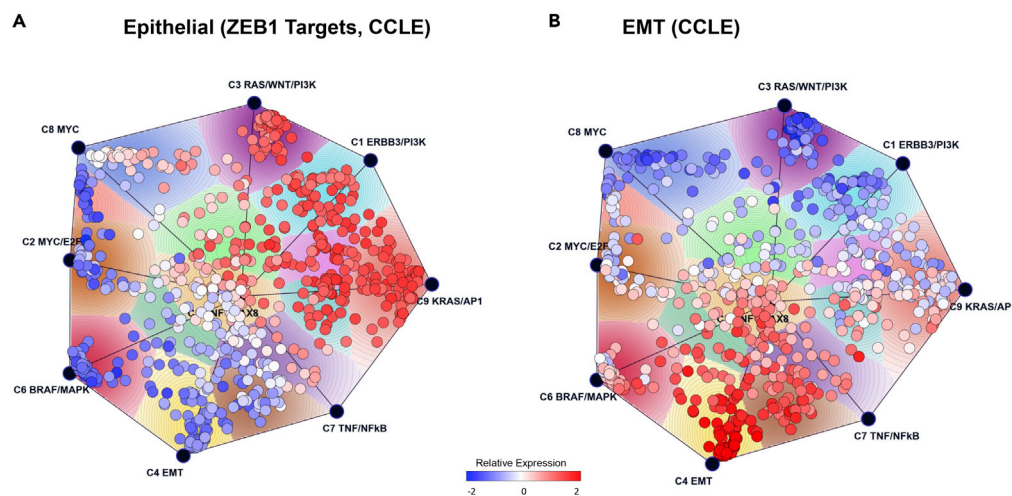


Figure 4. Onco-GPS Maps Showing that the Cyclin E CNA Signature Is Consistent with Activation of Epithelial Target Genes and Repression of Gene Sets Associated with the Epithelial-Mesenchymal Transition (EMT)

Same map as in Figure 3A but with samples color-coded to show the expression of an epithelial (ZEB1 targets) (A) and an EMT gene sets (B) (Groger et al., 2012).

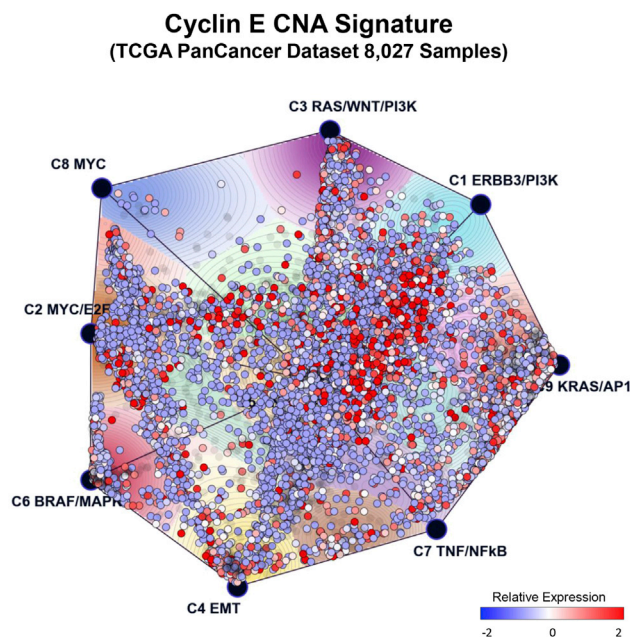


Figure 5. Onco-GPA Map of the Cyclin E CNA Signature Projected onto the Pan-cancer TCGA Dataset

Same Onco-GPS map as in Figure 3A but projecting 8,029 samples from the Pan-cancer TCGA dataset. The samples are color coded according to the expression of the cyclin E CNA signature.

In addition, copy number losses were detected for segments containing tumor suppressive microRNAs (miRNAs), miR33B, 151A, and 1288 (Gorringe et al., 2009; Xu et al., 2014; Yeh et al., 2016). To determine whether *c-Myc* copy number gain is reflected by increased *c-Myc* transcription and activation of downstream targets, we compared *c-Myc* transcript levels in the 12 clones that had been subjected to transient cyclin E overexpression (Figure 6C) and expression of gene sets known to be under *c-Myc* control (Figure 6D). Clearly *c-Myc* is expressed at higher levels in the two clones capable of anchorage-independent growth, and this has biological consequences in that downstream *c-Myc* targets are also expressed at higher levels in these clones.

Of 12 clones, 4 were found to be more resistant than the parental cell line to apoptosis resulting from treatment with the topoisomerase inhibitor, etoposide (Figure S3). These data indicate that, in an epithelial cell line expressing hTERT and partially compromised for p53 function, CNA alterations produced by transient cyclin E overexpression can promote specific oncogenic properties.

An Unbiased Grouping of Cancer Cell CNA Signatures Reveals a Strong Match with the Cyclin E Signature

To determine whether the cyclin E CNA signature is a global CNA pattern that could have been detected by an unbiased bioinformatics global analysis of CNA alterations, we carried out a Non-negative Matrix Factorization (Brunet et al., 2004; Kim et al., 2017; Tamayo et al., 2007) analysis of the CCLE copy number dataset to define global CNA signatures. For this analysis we define separate amplification and deletion binary features using as threshold a factor of two (half) for amplifications (deletions). This analysis produced 30 distinct CNA signatures, one of which (S7) showed a very strong association with the cyclin E CNA signature (Figure 7). Indeed, many of the cell lines that have high S7 CNA signature have also a strong association with the cyclin E CNA signature and are differentiated epithelial cell lines, mostly of ovarian and breast origin. The association scores for the cyclin E and S7 signatures are shown for the highest scoring cell lines and are shown in Table S2. We then ranked the CNA S7 signature features based on their degree of association with cyclin E CNA signature features (Table S3). Interestingly, we found that the principal driver of CNA signature S7 and cyclin E CNA signature association is a series of deletions in chromosome 18q12-23. These deletions dominate the S7 signature and are also dominant in the cyclin E signature (note the high levels of significance in Figure 1B). These data, taken together, suggest that deletions in the q arm of

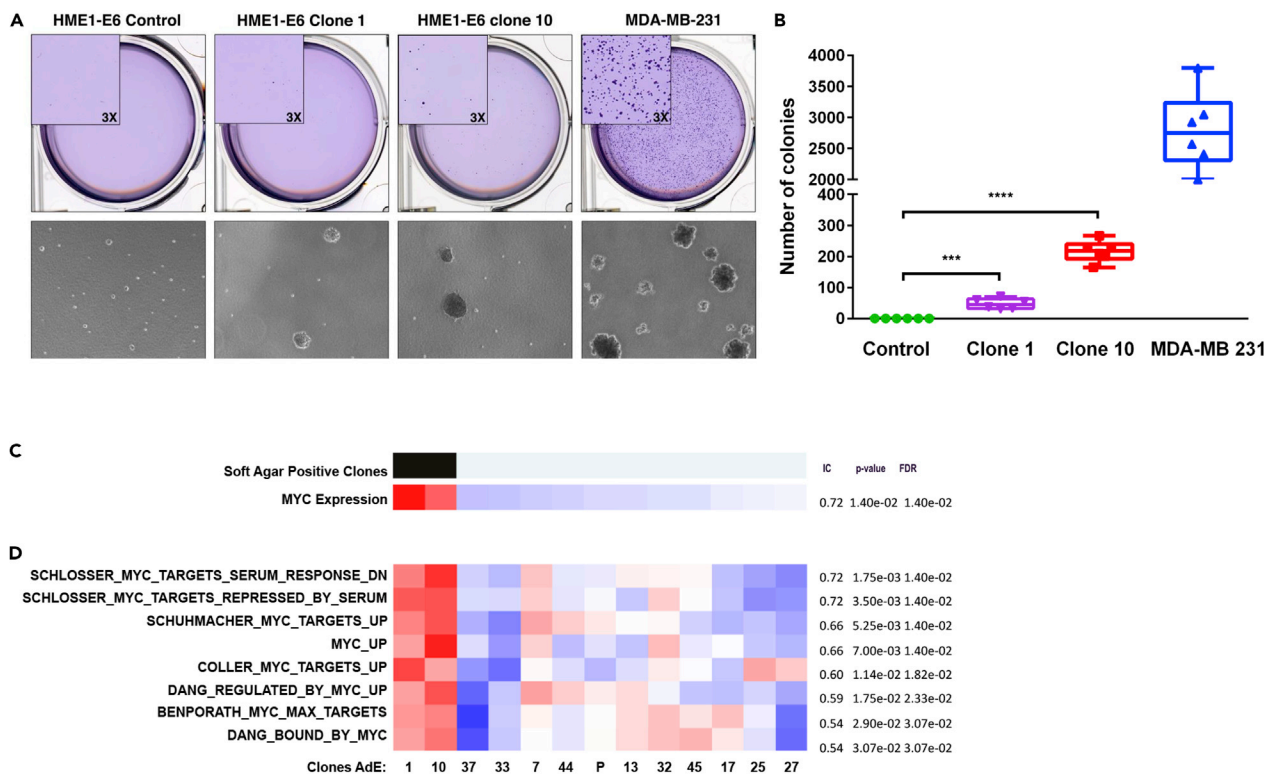


Figure 6. Two Clones Subjected to Transient Cyclin E Overexpression Are Capable of Anchorage-Independent Growth

(A) Low- (top) and high- (bottom) magnification images of parental cell line HME1-E6, derivative clones 1 and 10, and positive control breast cancer cell line MDA-MB-231 after plating in soft agar (scale bars, 50 μ m).

(B) Quantification of the number of measurable colonies (>50 μ m) formed in each cell line. Asterisks indicate statistically significant changes as determined by untailed t test (***) $p < 0.001$; (****) $p < 0.0001$. All the values represent the mean \pm SD from six independent experiments.

(C) Quantification of c-Myc transcript levels in the 12 clones.

(D) Quantification of transcript levels of genes trans activated by c-Myc. "P" refers to the parental cell lines HME1-E6. Statistical significance of top-scoring features was assessed by an empirical permutation test, and its corresponding null distribution, false discovery rates (FDR) plus bootstrap estimates of the association metric confidence intervals.

chromosome 18 are an important feature of differentiated epithelial cancers, particularly of the ovary and breast.

The Cyclin S7-cyclin E CNA Signature Drives Expected Transcriptional Alterations

The most likely manner in which CNAs can have a biological impact is to alter transcriptional output, where gene expression would be reduced on deleted chromosomal segments and increased on amplified segments. To test this hypothesis on a large dataset, we compared transcriptional amplitude to CNA status for cell lines in the CCLE. We determined whether the total CNA landscape associated with cyclin E overexpression confers the expected transcriptional modulation, by analyzing transcriptional amplitude in amplified and deleted chromosomal regions, respectively (Figure 8). As in Figure 2A, CCLE cell lines are arranged according to their cyclin E CNA signature score from left to right. The top analysis shows the cumulative expression level of genes on amplified chromosomal segments, whereas the bottom analysis shows the cumulative expression level of genes on deleted segments. As can be seen in Figure 8, in cell lines that strongly conform to the cyclin E CNA signature, there is a significant association between higher levels of transcription in amplified regions (IC = 0.329, p value = 0.004, false discovery rate [FDR] = 0.009) and, to an even greater degree, lower levels of transcription in deleted regions (IC = -0.513, p value = 0.0005, FDR = 0.001). In addition, assessment of transcriptional levels of individual genes in these regions also showed that, in most cases, there were strong concordances between deletion or amplification at these loci and reduced or increased transcription, respectively (Figure S4). One can therefore conclude that CNA changes in cells impact cellular biology, at least in part, by driving corresponding transcriptional changes.

Cyclin E Signature vs. 30 Global CNA Signatures

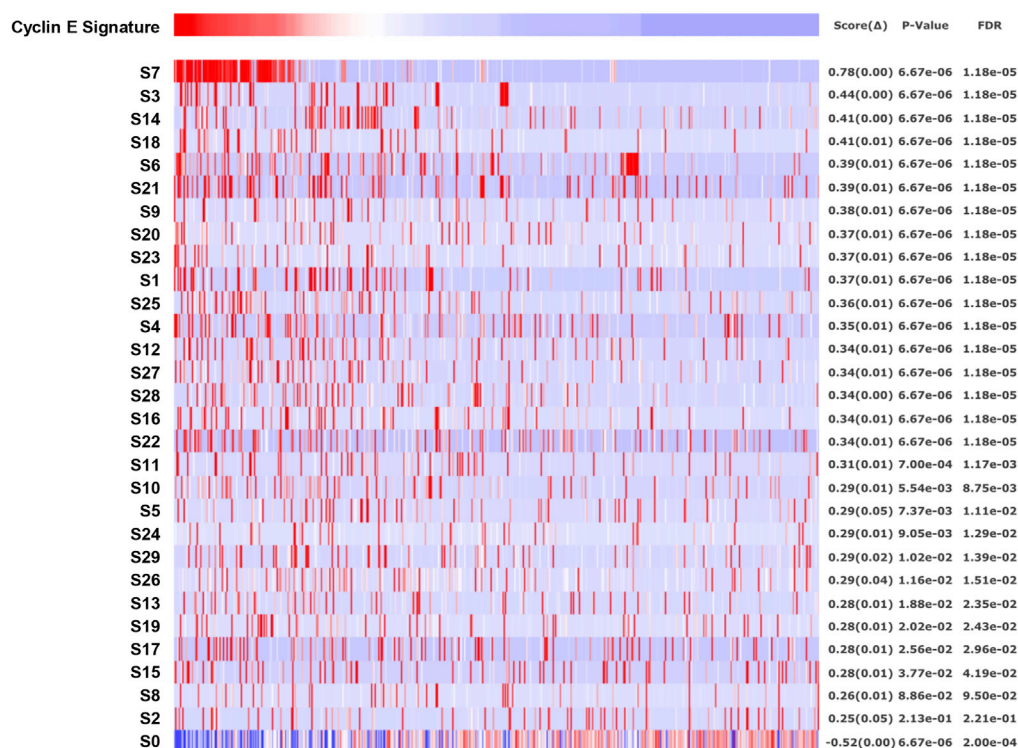


Figure 7. Comparison of the Cyclin E CNA Signature to 30 Global CNA Signatures across 1,030 Cancer-Derived Cell Lines

Top bar in the heat maps shows the high-to-low sorted amplitude of the cyclin E CNA signature across 1,030 cell lines in the CCLE dataset. The heatmap shows the amplitude of each of the 30 global CNA signatures. As can be seen in the figure, signature S7 is the best match. Statistical significance of top-scoring features was assessed by an empirical permutation test, and its corresponding null distribution, false discovery rates (FDR) plus bootstrap estimates of the association metric confidence intervals.

DISCUSSION

Our studies have demonstrated that cyclin E-mediated replication stress, by impairing replication of genomic regions and thereby leading to subsequent deletions and amplifications, promotes a state that has characteristics similar to differentiated epithelial cancers. This is based on a number of criteria, including pathway and protein expression data, as well as direct comparison of CNA signature patterns. The latter analysis has indicated that deletions on the q arms of chromosomes 17 and 18 are the most critical components of the association between the cyclin E signature and the signature characteristic of an un-biased grouping of cancer cells that best matches with the cyclin E signature. It is interesting to note that several tumor suppressor genes have been specifically mapped to this region, possibly explaining the relevance of this signature to tumorigenesis (Dellas et al., 2002; Takei et al., 1998; Thiagalingam et al., 1996; Yokota et al., 1997). We furthermore showed that expression of most genes in this region was reduced in cells containing these deletions, as expected, also likely contributing to the cancer phenotype.

Another interesting finding of this work is that after transient cyclin E expression and clonal expansion, subsets of clones were found capable of anchorage-independent growth and resistant to apoptosis, respectively. Although these properties are not synonymous with transformation, they are components of the cancer phenotype. The most likely driver of anchorage-independent growth in this context is a copy number gain of a segment of chromosome 8 containing *c-Myc* (Lyn-Cook et al., 1990; Telang et al., 1990; Valverius et al., 1990). In fact, the clearest demonstration that CNAs can have a direct impact on cellular biology came from comparing transcriptional profiles of the clones. The two clones that were capable of anchorage-

Cyclin E CNV and Expression Signatures

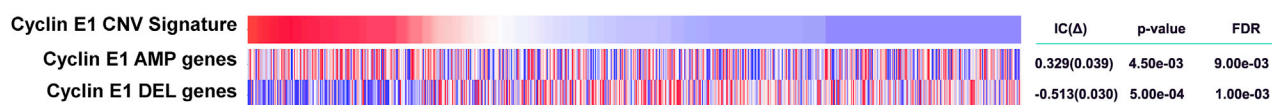


Figure 8. The S7 CNA Signature Produces a Parallel Transcriptional Signature

Top bar in the heatmaps shows the high-to-low sorted amplitude of the cyclin E CNA signature across 958 cell lines in the CCLE dataset. The second bar shows combined expression of genes in intervals showing copy number gains in the cyclin E signature, whereas the third bar shows combined expression of gene in the intervals showing copy number losses. Red represents higher levels of transcription, whereas blue represents lower levels. Statistical significance of top-scoring features was assessed by an empirical permutation test, and its corresponding null distribution, false discovery rates (FDR) plus bootstrap estimates of the association metric confidence intervals.

independent growth and showed CNA gains of a segment that included *c-Myc* showed increased levels not only of *c-Myc* transcripts but also of transcripts of known downstream targets of *c-Myc*. Since only two of twelve clones subjected to cyclin E overexpression contained this CNA, it is too soon to assign it to the overall cyclin E CNA signature or even to be considered statistically significant. Screening a larger number of clones for anchorage-independent growth and analyzing the associated CNAs will likely answer this question.

Our study only characterized one of many possible types of genomic and genetic alterations promoted by the oncoprotein cyclin E, specifically CNAs that could be detected using array technology. However, it is likely that much additional information could be gleaned by carrying out a more detailed analysis of clonal populations that had been subjected to cyclin E overexpression. Recently, a detailed study of the mutational landscape promoted by expression of p21^{Cip1} in a p53-deficient environment, another situation that promotes genetic and genomic instability, was published (Galanos et al., 2018). By analysis of the end products of the mutational process, the authors were able to deduce that an aberrant repair process was induced under these specific circumstances, suggesting a novel therapeutic target for malignancies with similar characteristics. It will be interesting to determine whether the repair response to damage produced by cyclin E overexpression is altered and whether this information might be used to identify new therapeutic targets.

The most important conclusion of this work is that oncogene generated CNA signatures are likely to be a useful parameter for characterizing tumors and cancer cells. The convergence of a simple *in vitro* model with patterns derived from the *in vivo* endpoints of oncogenesis suggests a model where oncoprotein-driven CNA patterns serve as a platform from which further genetic and epigenetic changes favorable for tumor formation can be selected. This hypothesis can be tested by determining the efficacy of the clones described here to form tumors in mouse xenograft models.

Limitations of the Study

In this study we show that transient overexpression of cyclin E in mammary epithelial cells produces a pattern of chromosomal CNAs that resembles those found in a subset of epithelial lineage cancers. This raised the question of whether these CNAs translate into changes in gene expression that would drive cancer biology. To address this, we analyzed how these particular CNAs in a large database of cancer cells translated to changes in gene expression and showed that deletions and amplifications produced decreased and increased expression, respectively, as hypothesized (Figures 8 and S4). We further showed that individual clones in our study that exhibited *c-Myc* amplification actually expressed elevated levels of *c-Myc* and transcriptional activation *c-Myc* downstream targets (Figures 6C and 6D). However, we did not carry out a more global analysis of the relationship between CNAs and gene expression in the individual clones. This study was not carried out at this time because of the small sample size available and therefore insufficient power to draw reliable conclusions. However, we consider elucidating the link between cyclin E-generated CNAs and gene expression in the context of cancer biology to be extremely important and plan to carry out such a study after analyzing a larger number of clones.

METHODS

All methods can be found in the accompanying [Transparent Methods supplemental file](#).

SUPPLEMENTAL INFORMATION

Supplemental Information can be found online at <https://doi.org/10.1016/j.isci.2019.08.043>

ACKNOWLEDGMENTS

This project was supported by the following United States National Institutes of Health grants: R01CA078343 (S.I.R.), R01GM074024, U24CA194107, R01HG009285, U54CA209891, R01CA172513, U24CA220341 (P.T.), U01CA217885 (W.K. and P.T.), and UL1 TR002550 (N.W.).

AUTHOR CONTRIBUTIONS

S.I.R. and S.G. conceived of the biological experiments. S.G. carried out the biological experiments. N.W. carried out CNA call analysis of the chromosomal microarray data. P.T. and W.K. conceived of and carried out the bioinformatic analyses. S.G., S.I.R., and P.T. wrote the manuscript. S.I.R. supervised the project.

DECLARATION OF INTERESTS

The authors declare that they have no financial interests related to this work.

Received: March 12, 2019

Revised: July 3, 2019

Accepted: August 21, 2019

Published: September 27, 2019

REFERENCES

- Barretina, J., Caponigro, G., Stransky, N., Venkatesan, K., Margolin, A.A., Kim, S., Wilson, C.J., Lehár, J., Kryukov, G.V., Sonkin, D., et al. (2012). The Cancer Cell Line Encyclopedia enables predictive modelling of anticancer drug sensitivity. *Nature* 483, 603–607.
- Bartkova, J., Rezaei, N., Liontos, M., Karakaidos, P., Kletsas, D., Issaeva, N., Vassiliou, L.V., Kolettas, E., Niforou, K., Zoumpourlis, V.C., et al. (2006). Oncogene-induced senescence is part of the tumorigenesis barrier imposed by DNA damage checkpoints. *Nature* 444, 633–637.
- Bortner, D.M., and Rosenberg, M.P. (1997). Induction of mammary gland hyperplasia and carcinomas in transgenic mice expressing human cyclin E. *Mol. Cell. Biol.* 17, 453–459.
- Brunet, J.-P., Tamayo, P., Golub, T.R., and Mesirov, J.P. (2004). Metagenes and molecular pattern discovery using matrix factorization. *Proc. Natl. Acad. Sci. U S A* 101, 4164–4169.
- Dellas, A., Torhorst, J., Schultheiss, E., Mihatsch, M.J., and Moch, H. (2002). DNA sequence losses on chromosomes 11p and 18q are associated with clinical outcome in lymph node-negative ductal breast cancer. *Clin. Cancer Res.* 8, 1210–1216.
- Galanos, P., Pappas, G., Polyzos, A., Kotsinas, A., Svolaki, I., Giakoumakis, N.N., Glytsou, C., Pateras, I.S., Swain, U., Souliotis, V.L., et al. (2018). Mutational signatures reveal the role of RAD52 in p53-independent p21-driven genomic instability. *Genome Biol.* 19, 37.
- Gorringe, K.L., Ramakrishna, M., Williams, L.H., Sridhar, A., Boyle, S.E., Bearfoot, J.L., Li, J., Anglesio, M.S., and Campbell, I.G. (2009). Are there any more ovarian tumor suppressor genes? A new perspective using ultra high-resolution copy number and loss of heterozygosity analysis. *Genes Chromosomes Cancer* 48, 931–942.
- Groger, C.J., Grubinger, M., Waldhor, T., Vierlinger, K., and Mikulits, W. (2012). Meta-analysis of gene expression signatures defining the epithelial to mesenchymal transition during cancer progression. *PLoS One* 7, e51136.
- Joe, H. (1989). Relative entropy measures of multivariate dependence. *J. Am. Stat. Assoc.* 84, 157.
- Kim, J.W., Abudayyeh, O.O., Yeerna, H., Yeang, C.-H., Stewart, M., Jenkins, R.W., Kitajima, S., Konieczkowski, D.J., Medetgul-Ernar, K., Cavazos, T., et al. (2017). Decomposing oncogenic transcriptional signatures to generate maps of divergent cellular states. *Cell Syst.* 5, 105–118.e9.
- Kim, J.W., Botvinnik, O.B., Abudayyeh, O., Birger, C., Rosenbluh, J., Shrestha, Y., Abazeed, M.E., Hammerman, P.S., DiCara, D., Konieczkowski, D.J., et al. (2016). Characterizing genomic alterations in cancer by complementary functional associations. *Nat. Biotechnol.* 34, 539–546.
- Lawrence, M.S., Stojanov, P., Mermel, C.H., Robinson, J.T., Garraway, L.A., Golub, T.R., Meyerson, M., Gabriel, S.B., Lander, E.S., and Getz, G. (2014). Discovery and saturation analysis of cancer genes across 21 tumour types. *Nature* 505, 495–501.
- Liberzon, A. (2014). A description of the molecular signatures database (MSigDB) web site. *Methods Mol. Biol.* 1150, 153–160.
- Liberzon, A., Birger, C., Thorvaldsdóttir, H., Ghandi, M., Mesirov, J.P., and Tamayo, P. (2015). The Molecular Signatures Database (MSigDB) hallmark gene set collection. *Cell Syst.* 1, 417–425.
- Liberzon, A., Subramanian, A., Pinchback, R., Thorvaldsdóttir, H., Tamayo, P., and Mesirov, J.P. (2011). Molecular signatures database (MSigDB) 3.0. *Bioinformatics* 27, 1739–1740.
- Lyn-Cook, B.D., Siegal, G.P., and Kaufman, D.G. (1990). Malignant transformation of human endometrial stromal cells by transfection of c-myc: effects of pRSVneo cotransfection and treatment with MNNG. *Pathobiology* 58, 146–152.
- Porter, P.L., Malone, K.E., Heagerty, P.J., Alexander, G.M., Gatti, L.A., Firpo, E.J., Daling, J.R., and Roberts, J.M. (1997). Expression of cell-cycle regulators p27Kip1 and cyclin E, alone and in combination, correlate with survival in young breast cancer patients. *Nat. Med.* 3, 222–225.
- Smith, A.P., Henze, M., Lee, J.A., Osborn, K.G., Keck, J.M., Tedesco, D., Bortner, D.M., Rosenberg, M.P., and Reed, S.I. (2006). Deregulated cyclin E promotes p53 loss of heterozygosity and tumorigenesis in the mouse mammary gland. *Oncogene* 25, 7245–7259.
- Spruck, C.H., Won, K.A., and Reed, S.I. (1999). Deregulated cyclin E induces chromosome instability. *Nature* 401, 297–300.
- Takei, K., Kohno, T., Hamada, K., Takita, J., Noguchi, M., Matsuno, Y., Hirohashi, S., Uezato, H., and Yokota, J. (1998). A novel tumor suppressor locus on chromosome 18q involved in the development of human lung cancer. *Cancer Res.* 58, 3700–3705.
- Tamayo, P., Scanfeld, D., Ebert, B.L., Gillette, M.A., Roberts, C.W.M., and Mesirov, J.P. (2007). Metagene projection for cross-platform, cross-species characterization of global transcriptional states. *Proc. Natl. Acad. Sci. U S A* 104, 5959–5964.
- Teixeira, L.K., Wang, X., Li, Y., Ekholm-Reed, S., Wu, X., Wang, P., and Reed, S.I. (2015). Cyclin E

deregulation promotes loss of specific genomic regions. *Curr. Biol.* 25, 1327–1333.

Telang, N.T., Osborne, M.P., Sweterlitsch, L.A., and Narayanan, R. (1990). Neoplastic transformation of mouse mammary epithelial cells by deregulated myc expression. *Cell Regul.* 1, 863–872.

Thiagalingam, S., Lengauer, C., Leach, F.S., Schutte, M., Hahn, S.A., Overhauser, J., Willson, J.K., Markowitz, S., Hamilton, S.R., Kern, S.E., et al. (1996). Evaluation of candidate tumour suppressor genes on chromosome 18 in colorectal cancers. *Nat. Genet.* 13, 343–346.

Thomas, M., Pim, D., and Banks, L. (1999). The role of the E6-p53 interaction in the molecular pathogenesis of HPV. *Oncogene* 18, 7690–7700.

Valverius, E.M., Ciardiello, F., Heldin, N.E., Blondel, B., Merlo, G., Smith, G., Stampfer, M.R., Lippman, M.E., Dickson, R.B., and Salomon, D.S. (1990). Stromal influences on transformation of human mammary epithelial cells overexpressing c-myc and SV40T. *J. Cell Physiol.* 145, 207–216.

Wang, Z., Jensen, M.A., and Zenklusen, J.C. (2016). A practical guide to the cancer genome atlas (TCGA). *Methods Mol. Biol.* 1418, 111–141.

Xu, N., Li, Z., Yu, Z., Yan, F., Liu, Y., Lu, X., and Yang, W. (2014). MicroRNA-33b suppresses migration and invasion by targeting c-Myc in osteosarcoma cells. *PLoS One* 9, e115300.

Yeh, T.C., Huang, T.T., Yeh, T.S., Chen, Y.R., Hsu, K.W., Yin, P.H., Lee, H.C., and Tseng, L.M. (2016). miR-151-3p Targets TWIST1 to repress migration of human breast cancer cells. *PLoS One* 11, e0168171.

Yokota, T., Matsumoto, S., Yoshimoto, M., Kasumi, F., Akiyama, F., Sakamoto, G., Nakamura, Y., and Emi, M. (1997). Mapping of a breast cancer tumor suppressor gene locus to a 4-cM interval on chromosome 18q21. *Jpn. J. Cancer Res.* 88, 959–964.

ISCI, Volume 19

Supplemental Information

Cyclin E Overexpression in Human Mammary

Epithelial Cells Promotes Epithelial

Cancer-Specific Copy Number Alterations

Servando Giraldez, Pablo Tamayo, Nathan Wineinger, William Kim, and Steven I. Reed

Supplemental Information

Transparent Methods

Cell lines. hTERT-HME1 (ATCC, CRL-4010), an immortalized human mammary epithelial cell derived from the mammary glands of a healthy donor and hTERT-HME1-E6, an hTERT-HME1 derivative cell line constitutively expressing the human papilloma virus protein E6 (HPV-E6), were grown in MCDB 131 medium (Gibco) supplemented with 70 µg/mL bovine pituitary extract (Hammond Cell Tech), 1% newborn calf serum (Gemini Bio-Products), 5 µg/mL holotransferrin (Sigma), 10 ng/mL human epidermal growth factor (Invitrogen), 0.5 µg/mL hydrocortisone (Sigma), 5 µg/mL insulin (Sigma), 2 mM L-glutamine (Gibco), 100 U/mL penicillin (Gibco), and 100 µg/mL streptomycin (Gibco). MDA-MB-231 (ATCC, HTB-26), was originally grown in Leibovitz's L-15 medium (Gibco) supplemented with 10% newborn calf serum (Gemini Bio-Products), 100 U/mL penicillin, and 100 µg/mL streptomycin. To carry out the anchorage independent growth assays, MDA-MB-231 cells were slowly conditioned, over several passages using increasing amounts of the MCDB 131 medium and decreasing amounts of the Leibovitz's L-15 medium, to grow in the same medium as HME1 cells. The HEK-293A cell line was grown in DMEM medium (Gibco) supplemented with 10% newborn calf serum (Gemini Bio-Products), 2 mM L-glutamine (Gibco), 100 U/mL penicillin (Gibco), and 100 µg/mL streptomycin (Gibco). The HEK293FT cell line was grown as described for HEK293A but with 500 µg/mL Geneticin selective antibiotic, as recommended by the manufacturer. Cells were maintained in a humidified 37 °C incubator with 5% CO₂.

Viral transductions. Recombinant lentivirus expressing the Herpesvirus E6 protein (HPV-E6) fused to a hemagglutinin (HA) tag was produced in HEK293 FT cell line. Cells were transfected using Xfect reagent (Clontech) with the plasmids: pLentiN 18E6no* a gift from Karl Munger (Addgene plasmid # 37446) (Spangle et al., 2012) and pMD2-G, pMDLg-PRRE and pRSV-Rev a gift from Didier Trono (Addgene plasmid # 12259, # 12251 and # 12253, respectively) (Dull et al.,

1998). After 48h of transfection, cell supernatant was harvested and passed through a 0.45 μm Puradisc 25 mm filter. Subsequently, viruses were concentrated using a Lenti-X-concentrator (Clontech). HME1 cells were transduced with lentivirus-containing supernatant for 24h, and transduced cells were selected after seven days in 10 $\mu\text{g}/\text{ml}$ Blasticidin (Gibco).

Recombinant adenovirus expressing Green Fluorescent Protein (Ad-GFP) obtained from Vector Biolabs and recombinant adenovirus expressing the cyclin E cDNA (Ad-CycE)(Ekholm-Reed et al., 2004) were amplified in HEK-293A cells and purified by ultracentrifugation on a CsCl gradient. HME1-E6 cells were transduced with Ad-GFP or Ad-Cyc E three times per week during two weeks at 48-hour intervals. Single live cells were sorted into 96-wells plates 48 hours after the sixth transduction using a FACSAria (BD Biosciences). Sorted cells were cultured and amplified into populations of approximately 10 million derivatives, and then analyzed and frozen down for further studies.

Western Blotting. HME1 and HME1-E6 dividing cells were harvested and total cell extracts prepared in cold lysis buffer as described previously (Teixeira et al., 2015). Antibodies used were mouse monoclonal anti-cyclin E (HE12, Santa Cruz Biotechnology), mouse monoclonal anti-HA-Peroxidase (Roche) and rabbit polyclonal anti-GAPDH (ProSci).

Apoptosis Assay. HME1 and HME1-E6 cells were incubated with the topoisomerase inhibitor etoposide (Sigma; 10 μM) and the level of apoptosis was determined by Western blotting to monitor the appearance of cleaved-PARP at 8, 12, 24 and 48 hours after treatment or for comparative analysis of individual clone and HME1-E6 48 hours. Antibodies used were rabbit polyclonal anti-Cleaved-PARP (Cell signaling), mouse monoclonal anti-p53 (DO1, Santa Cruz Biotechnology) and rabbit polyclonal anti-GAPDH (ProSci). In addition, the level of apoptosis activation was measured by Annexin V staining. HME1 and HME1-E6 were cultured in twelve

wells plates and incubated with DMSO or 10 μ M etoposide, as well as Incucyte annexin V red reagent (Essen BioScience). After 24 hours, cells were fixed with methanol, stained with Dapi and analyzed for Annexin V staining using a Keyence BZX700 all-in-one fluorescence microscope.

Real-time PCR. Total DNA from HME1-E6 clonal populations was extracted using QIAmp[®] DNA Mini kit (Qiagen). To test whether cyclin E overexpression had induced permanent genomic alterations in these clones at the specific regions described previously (Teixeira et al., 2015), real-time PCR reactions were carried out with iQ[™] Green Supermix (Bio-Rad) according to manufacturer's instruction. Each sample was run in quadruplicate on a Cromo4 real timePCR instrument (MJ Research) and analyzed using Opticon Monitor software (Bio-Rad). Primer sequences have been described previously (Teixeira et al., 2015). Copy Number Alteration (CNA) of specific genomic regions was determined by normalizing to the locus encoding α -tubulin and was determined using the formula: $CNA = 2Ct(\text{tubulin region}) - Ct(\text{specific region})$, where Ct is the cycle threshold. Relative CNAs were determined using the formula: cyclin E CNA/tubulin CNA.

Chromosomal Microarray Analysis (CMA). Total DNA purified from clonal populations was extracted as described in the previous section and was analyzed via CytoscanHD array analysis (Affymetrix). Raw CNA data was pre-processed using the affy2s package (Hernandez-Ferrer et al., 2015) in R using the CytoScanHD Array NA33 reference model and annotation database. B allele frequency values were input into PennCNV using the *hhal* hidden Markov model. PennCNV calls were used in downstream analyses. Copy number variable regions (CNVR) in each sample were defined after merging CNV calls within 1 Mb of a neighboring CNV. Association of each CNVR (using average copy number) with treatment and control groups was tested using Mann-Whitney U tests. Enrichment of associations across the genome was tested by comparing the resulting p-values to a uniform distribution using a one-sided KS test. All analyses were performed

in *R* (version 3.3.2).

Anchorage independent growth assay. 2×10^4 cells were cast in top layer medium composed of full growth medium and 0.3% SeaPlaque agarose (Cambrex, Rockland, ME, USA). The cell mixture was plated in 6-well plates on top of a solidified layer of 0.6% agarose and 2 x MCDB 131 growth medium and allowed to solidify. Images were acquired at 10x magnification using a LSM 710 laser scanning confocal microscope attached to an Observer Z1 microscope (Carl Zeiss). Colonies were photographed after 30 days of seeding and then stained with crystal violet 0.1%, diluted in 10% ethanol for 5 min, destained in water using a shaking platform. Colonies were quantified by manual counting.

Generation of the cyclin E CNA signature. We generate a cyclin E CNA signature score, cE_{sig} , for each cancer sample by performing a weighted sum of all the n cyclin E-induced gains and losses (Supplemental Table 1),

$$cE_{sig} = \sum_{i=0}^n CNA_i \times \log(1/p_i). \quad (1)$$

Where CNA_i is an indicator function equal to 1 if the sample has the i th cyclin E-induced copy number alteration and 0 otherwise. The p_i is the p-value for each copy number alteration (see Chromosomal Microarray Analysis above). The \log in the equation allows for a smooth weighting taking into account the statistical significance of each copy number alteration but without having the most significant ones over-dominate the score.

RNA preparation and analysis. Total RNA was extracted from actively dividing cells using the Quick RNA Zymo kit (Zymo Research) according to the manufacturer's instructions. Quality assessment of RNA samples were obtained using Nanodrop, agarose gel electrophoresis and

Agilent 2100. After the QC procedures, NebNext Ultra RNA (Illumina) was used for cDNA library generation. Briefly, mRNAs from each samples were enriched using oligo(dT) beads, fragmented randomly by adding fragmentation buffer, followed by cDNA synthesis using mRNA template and random hexamers primer, after which a custom second-strand synthesis buffer (Illumina), dNTPs, RNase H and DNA polymerase I were added to initiate the second-strand synthesis. After a series of terminal repair, A ligation and sequencing adaptor ligation, the double-stranded cDNA library was completed through size selection and PCR enrichment. QC of the resulting cDNA library was performed using Qubit 2.0, Agilent 2100, and Q-PCR. After QC and qualification, the resulting cDNA libraries were sequenced using Illumina Novaseq 6000 at read depth of between 2-40 million reads as PE150 reads. The resulting FASTQ files were processed by bcbio RNA-seq pipeline (Steinbaugh et al). Briefly, the raw reads were aligned to reference genome GRCh37 using STAR 2.6.1; Duplicated reads were marked by the bammarkduplicates module from biobambam 2.0.87; salmon 0.13.1 was then used for the transcript quantification.

To assess the top gene expression associated with anchorage-independent growth phenotype, we quantified the degree of association using an information-theoretic measure - the Information Coefficient (IC) and calculated an empirical permutation test for statistical significance (Kim et al., 2016). We also performed a systematic evaluation of more general gene sets that associate with the clones by performing ssGSEA using gene sets from the Molecular Signatures Database (MSigDB database, subcollections:C2, C6). Enrichment scores for the corresponding samples were calculated using single-sample GSEA (ssGSEA) projections of these cell type signatures (Barbie et al., 2009). Briefly, gene expression values in each individual sample were rank-normalized by their absolute expression, followed by calculation of an enrichment score by evaluating the differences in the empirical cumulative distribution functions of the genes in the gene set relative to the remaining genes. A positive enrichment score denotes significant overlap of the gene set with groups of genes at the top of the ranked list, while a negative

enrichment score denotes a significant overlap of the signature gene set with groups of genes at the bottom of the ranked list. Among the top matching gene sets, assessed by IC, we focused on multiple independent gene sets significantly enriched in the anchorage-independent growth clones that represent the Myc pathway.

Matching cyclin E CNA with expression. To evaluate corresponding changes of transcription of genes in the regions of CNA induced by cyclin E1, we focused on 19 genes which were either amplified or deleted and generated genesets of cycle E1 amplification or deletion and performed ssGSEA across the CCLE expression dataset. The degree of associations between cyclin E CNA signature score and ssGSEA scores of expression of cyclin E1 amplification and deletion were then assessed by calculating IC and an empirical permutation test for statistical significance. For assessment of individual genes, samples were binned based on the presence (amplification/deletion) or absence(wild-type) of these lesions, and t-test was conducted on the expression median expression values in each group.

Data and Software Availability. The accession number for the CMA primary data is NCBI GEO: GSE136297. The accession number for the RNASeq data is NCBI GEO: GSE136078.

Barbie, D.A., Tamayo, P., Boehm, J.S., Kim, S.Y., Moody, S.E., Dunn, I.F., Schinzel, A.C., Sandy, P., Meylan, E., Scholl, C., *et al.* (2009). Systematic RNA interference reveals that oncogenic KRAS-driven cancers require TBK1. *Nature* **462**, 108-112.

Dull, T., Zufferey, R., Kelly, M., Mandel, R.J., Nguyen, M., Trono, D., and Naldini, L. (1998). A third-generation lentivirus vector with a conditional packaging system. *J Virol* **72**, 8463-8471.

Ekholm-Reed, S., Mendez, J., Tedesco, D., Zetterberg, A., Stillman, B., and Reed, S.I. (2004). Deregulation of cyclin E in human cells interferes with prereplication complex assembly. *J Cell Biol* **165**, 789-800.

Hernandez-Ferrer, C., Quintela Garcia, I., Danielski, K., Carracedo, A., Perez-Jurado, L.A., and Gonzalez, J.R. (2015). *affy2sv*: an R package to pre-process Affymetrix CytoScan HD and 750K arrays for SNP, CNV, inversion and mosaicism calling. *BMC Bioinformatics* **16**, 167.

Kim, J.W., Botvinnik, O.B., Abudayyeh, O., Birger, C., Rosenbluh, J., Shrestha, Y., Abazeed, M.E., Hammerman, P.S., DiCara, D., Konieczkowski, D.J., *et al.* (2016). Characterizing genomic alterations in cancer by complementary functional associations. *Nat Biotechnol* 34, 539-546.

Spangle, J.M., Ghosh-Choudhury, N., and Munger, K. (2012). Activation of cap-dependent translation by mucosal human papillomavirus E6 proteins is dependent on the integrity of the LXXLL binding motif. *J Virol* 86, 7466-7472.

Teixeira, L.K., Wang, X., Li, Y., Ekholm-Reed, S., Wu, X., Wang, P., and Reed, S.I. (2015). Cyclin E deregulation promotes loss of specific genomic regions. *Curr Biol* 25, 1327-1333.

Supplemental Figure 1, related to Figure 1. Characterization of the HME1 derivative HME1-E6. A.

Western blot of parental HME1 line and derivative HME1-E6, expressing HA-tagged human papillomavirus protein E6. Extracts were analyzed by SDS-PAGE and blotting. Relevant proteins are indicated.

Glyceraldehyde phosphae dehydrogenase (GAPDH) serves as a loading control. **B.** Time course of HME1 and HME1-E6 cells treated with the DNA damaging agent etoposide. Extracts were prepared at the indicated times and analyzed by SDS-PAGE and blotting. Relevant proteins are indicated. "C" represents untreated cells.

Glyceraldehyde phosphate dehydrogenase (GAPDH) serves as a loading control. **C.** Etoposide-treated HME1 and HME1-E6 were scored for apoptosis after 24 hours of treatment by staining with Annexin V. Data represents three experiments. Error bars correspond to SD. Statistical significance determined by untailed *t*-test. *, $p < 0.05$.

Supplemental Figure 2, related to Figure 6. Results of GWAS comparing clones capable of anchorage-independent growth with others. Heatmap shows chromosomal segments where difference occur.

Supplemental Figure 3, related to Figure 6. Four clones subjected to transient cyclin E

overexpression are resistant to apoptosis in response to treatment with etoposide. Apoptosis was scored based on levels of cleaved PARP. Lysates from the parental cell line and 4 clones showing reduced levels of cleaved PARP were analyzed by SDS-PAGE and western blotting (left). Quantification to 2 independent experiments is shown on the right. Bars represent cleaved PARP signal normalized to GAPDH. All lysates were prepared 48 hr after treatment with etoposide. Error bars correspond to SD.

Supplemental Figure 4, related to Figure 8. Transcriptional modulation of individual genes that drive

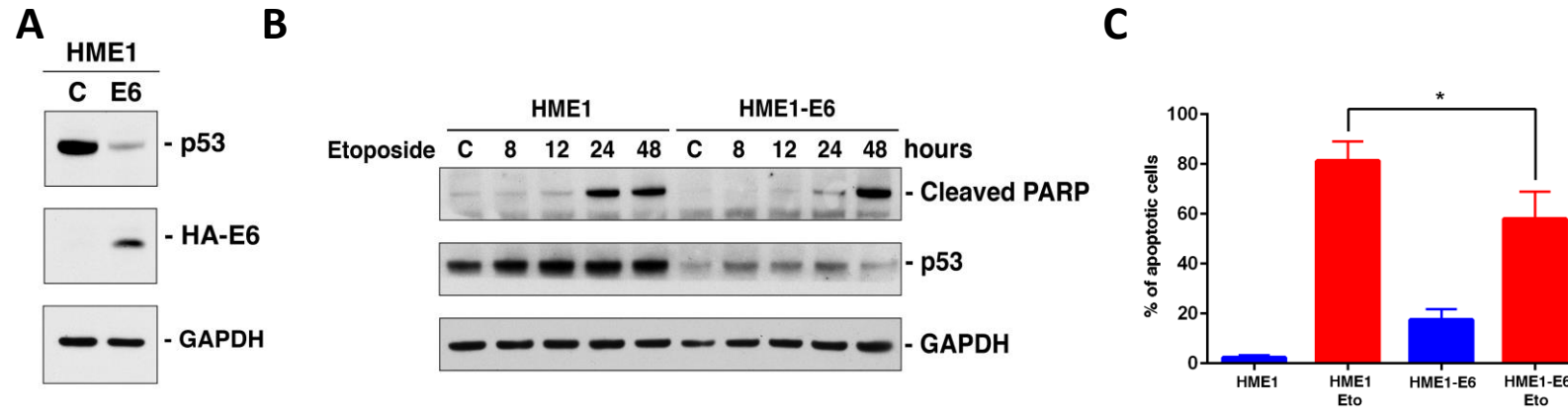
the cyclin E-S7 CNA signature. Plots of expression of genes in the chromosomal intervals that drive the cyclin E-S7 CNA signature. Data from 958 cell lines in the CCLE. "Wild-type" represents transcriptional amplitude data from cells that have a 2N DNA content at the queried locus whereas the other bar represents transcriptional amplitude at the indicated locus in cell lines that have CNA gains or losses, respectively.

Supplemental Table 1, related to Figure 1. CNA Call Analysis. Columns represent CNA data from individual clones with GFP control clones to the left and cyclin E experimental clones to the right. Numbers in each column represents signal amplitude, where “2” corresponds to the mean value for the control clones. Columns to the right are gene annotation and significance of cyclin E-specific differences from the control value. Rows are ordered according to the significance (p value) of difference between experimental and control clones.

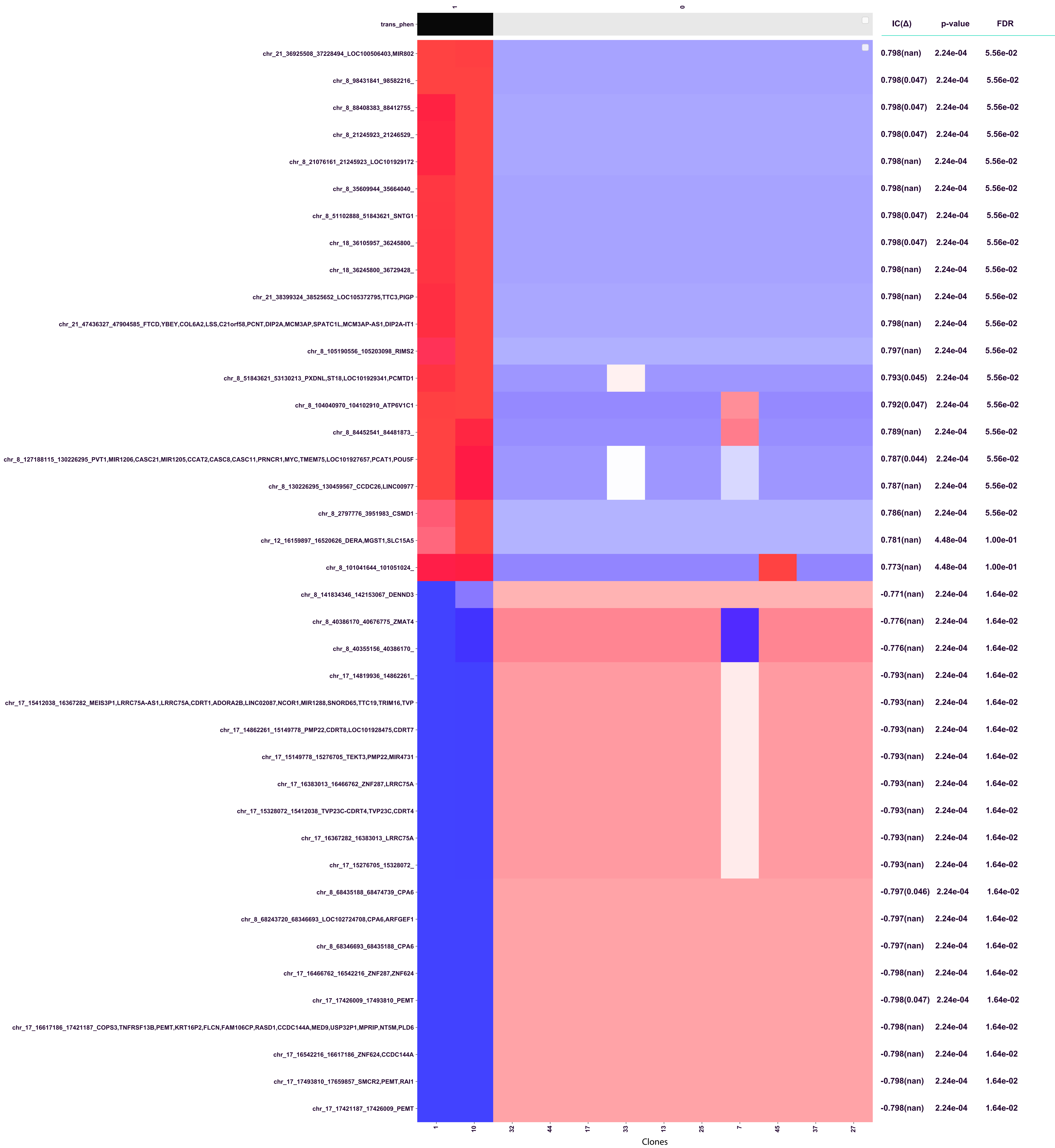
Supplemental Table 2, related to Figure 7. Association of Cancer Cell Lines with the Cyclin E CNA signature.

Supplemental Table 3, related to Figure 7. Features that associate the S7 signature with the cyclin E signature.

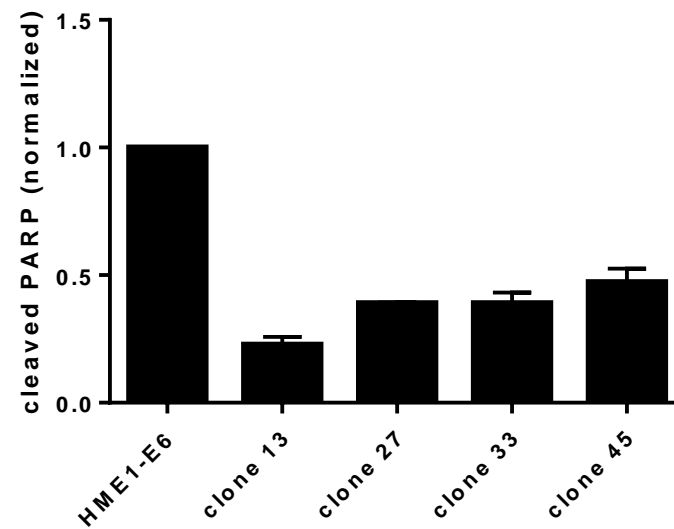
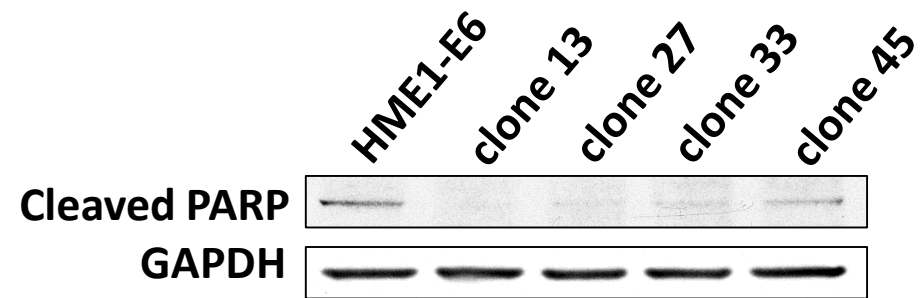
Supplemental Fig. 1.



Trans Phenotype vs Features

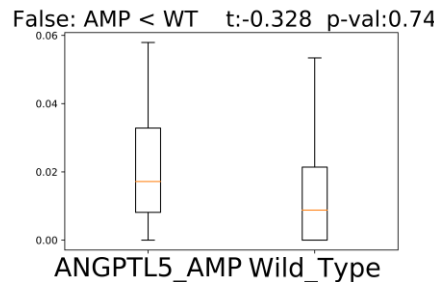


Supplemental Figure 3.

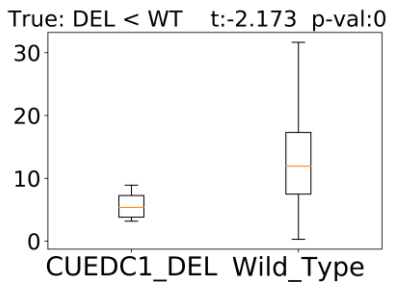


Supplemental Figure 4

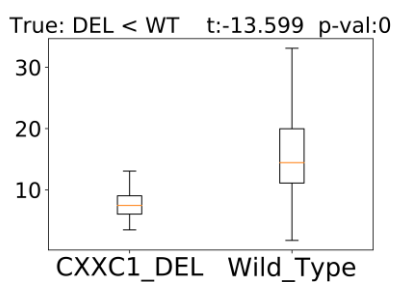
ANGPTL5 Expression



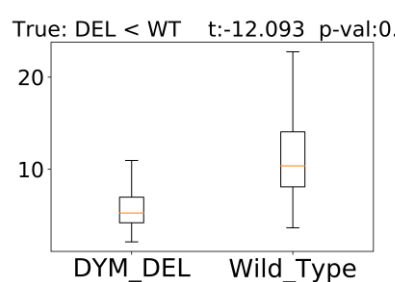
CUEDC1 Expression



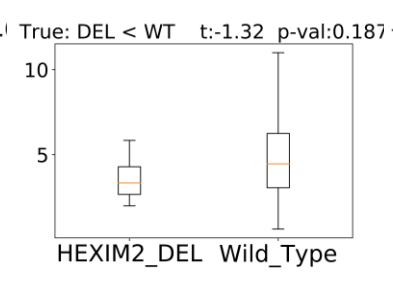
CXXC1 Expression



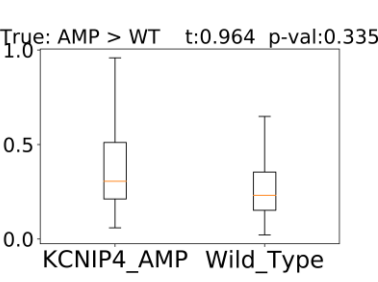
DYM Expression



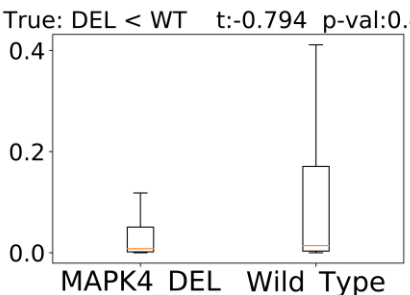
HEXIM2 Expression



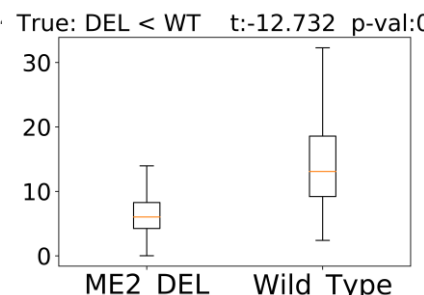
KCNIP4 Expression



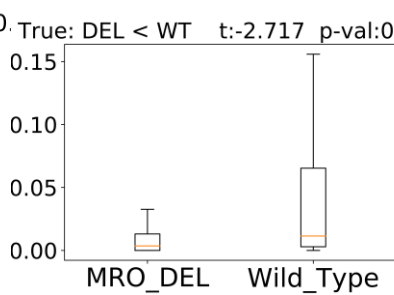
MAPK4 Expression



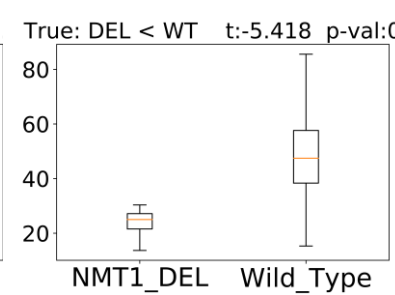
ME2 Expression



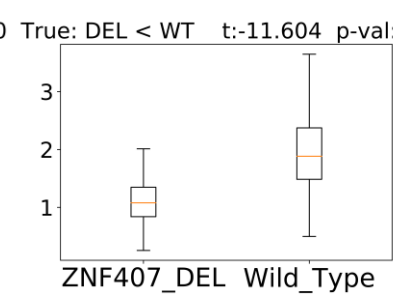
MRO Expression



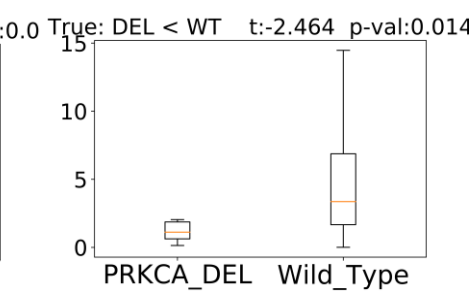
NMT1 Expression



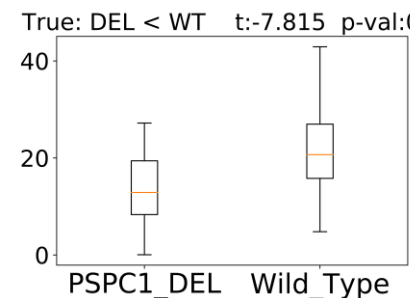
ZNF407 Expression



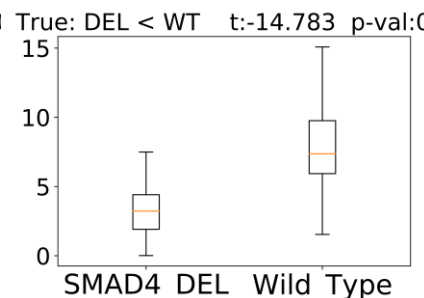
PRKCA Expression



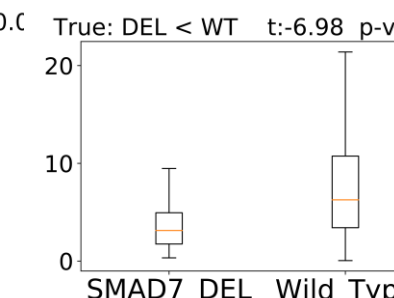
PSPC1 Expression



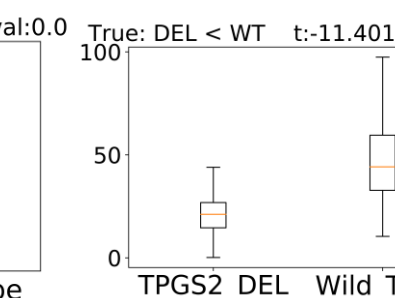
SMAD4 Expression



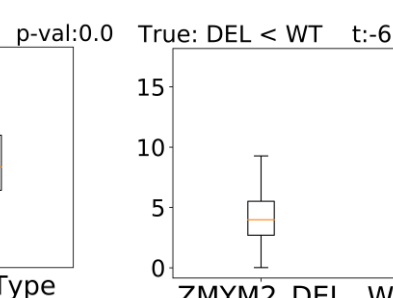
SMAD7 Expression



TPGS2 Expression



ZMYM2 Expression



Supplemental Table 3

rank in S7 gene (location) amplitude

68 ZNF407_DEL (18q23) 0.7331848802004938
75 MAPK4_DEL (18q21.1) 0.7297331514026538
77 CXXC1_DEL (18q12) 0.7295840007654858
88 ME2_DEL (18q21) 0.7276599860224345
96 MRO_DEL (18q21) 0.7251959319882806
117 SMAD4_DEL (18q21.1) 0.7169959039016859
120 DYM_DEL (18q21.1) 0.7103402404197144
122 SMAD7_DEL (18q21.1) 0.7077167978077717
170 TPGS2_DEL (18q12.2) 0.5642243087993831
172 MIR4318_DEL (18) 0.5571431228831131
564 KCNIP4_AMP (4p15.32) 0.025892746117716952
1189 PRKCA_DEL (17q22-q24) 0.014036884969398656
1290 CUEDC1_DEL (17q23.2) 0.013163903029006262
2404 PSPC1_DEL (13q11) 0.007262524209848104
2446 NMT1_DEL (17q21.31) 0.007198605859448572
3281 SPATA22_AMP (17p13.3) 0.005215061482637382
3788 ZMYM2_DEL (13q11-q12) 0.004130923527556818
3894 ANGPTL5_AMP (11q22.2) 0.00397549078811101
4135 USP6_AMP (17p13) 0.003480046146739011
5239 HEXIM2_DEL (17q21.31) 0.0018796616969080087

....